IET Inspec

Inspec Analytics

Uncover deeper insights into the impact of global research

Understand your place in the global engineering research landscape and make strategic decisions about the direction of your projects with a dynamic research intelligence tool based on the IET's renowned Inspec database.

Precision analytics for research excellence

Enhanced features allow you to uncover deeper insights into the impact of global research and explore the elements most valuable to you. With Inspec Analytics, you can:

–Deepen your understanding of global scientific trends.

–Define the scope of research initiatives to maximise your impact.

–Assess your organisation's research output and impact.

–Evaluate the success of collaborative partnerships.

Learn more at **inspec-analytics.theiet.org**

Received: 5 April 2021 | Revised: 7 August 2021 | Accepted: 3 September 2021

IET Power Electronics

DOI: 10.1049/pel2.12201

The Institution of Engineering and Technology WILEY

ORIGINAL RESEARCH PAPER

Modelling and performance evaluation of diode-assisted impedance source networks

Hamed Rezazadeh | **Mohammad Monfared** | **Ali Nikbahar**

Department of Electrical Engineering, Faculty of Engineering, Ferdowsi University of Mashhad, Mashhad, Iran

Correspondence
Mohammad Monfared, Ferdowsi University of Mashhad, Azadi Sq., Mashhad, Iran.
Email: m.monfared@um.ac.ir

Abstract

This paper deals with a family of two- and three-windings coupled inductor-based impedance source networks. They have been basically derived from the successful quasi-Y-source network (q-YSN) by replacing one of its capacitors with a diode with different combinations of coupled inductors and called diode assisted impedance source networks (DA-ISNs). The general three-windings version, called diode-assisted Y-source network (DA-YSN), as the origin of all other simplified versions, is thoroughly investigated from various points of view. From the voltage gain characteristics aspect, it offers a higher voltage gain with the same number of elements as the conventional q-YSN. Lower magnetizing and input current ripples show the higher power density of DA-YSN in comparison to q-YSN. The effectively reduced voltage stress and the total value of capacitors, and a considerable decreased conversion loss of the magnetic element are the other attractive features of DA-YSN. With the advantages of a low input current ripple and a high voltage gain, DA-ISNs can be suitable choices for renewable energy and distributed power generation systems. Operating principle, circuit analysis, and parameters design guidelines for DA-YSN are thoroughly investigated. Also, the small-signal modelling, analysis and the controller design are presented in this paper. Finally, the theoretical properties of DA-YSN are scrutinized by performing extensive experiments on a 200 W laboratory prototype.

1 | INTRODUCTION

Recently, various impedance source networks have been proposed for all power conversion applications, that is, AC-DC, DC-AC, DC-DC, and AC-AC. Adjustable speed drives [1, 2], uninterruptible power supplies [3, 4], renewable energy and distributed power generation systems [5–10], electric vehicles [11–13], and DC circuit breakers [14] are just some successful application proposals. Single-stage simultaneous step-up and step-down power conversion, as an attractive advantage of the impedance source networks, leads to enhanced reliability and improved performance of the power systems. Modelling, control, and modulation techniques are well investigated in some papers [15–19], while other researches are more focused on the improvement of circuit topologies. The diode/capacitor assisted [20], switched-capacitors/inductors [21–24], switched boost networks [25, 26], and voltage lift [27] are proposed to improve the voltage gain, reduce the components' voltage / current stress, and increase the power density. The magnetically coupled impedance source (MCIS) converters, as a recent topology improvement, offer a high voltage gain with a fewer number of elements and a shorter shoot-through duty cycle (D_{ST}) requirement. The Y–source network (YSN) [28], as the basic structure of the T-source, the Γ-source and the Flipped Γ-source networks [29], the Δ-source network [30], and the sigma-Z-source network [31], are some of the successful MCIS networks, all offering high voltage gains by proper utilization of the coupled inductor turn ratio as an added design flexibility. Nevertheless, they suffer from a discontinuous input current, which leads to a high current stress at the source side. To overcome this problem, the continuous input current impedance source networks are introduced, such as the quasi Y-source [32],

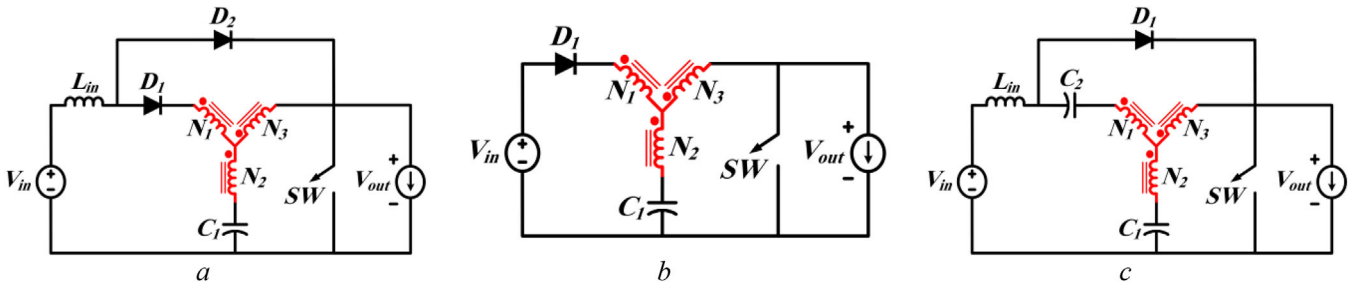

FIGURE 1 Y-shaped networks. (a) DA-YSN [38], (b) YSN [28], (c) q-YSN [32]

the quasi T-source, the quasi Γ-source, and the LCCT-Z-source networks, all proposed in [33], the A-source network [34], the quasi-Δ-source networks [35], and the quadratic-Δ-source network [36]. The quasi-Y-source network (q-YSN), as the origin of almost all the continuous input current MCIS networks, also offers a smaller magnetic core of the coupled inductor compared to the Y-source network (YSN). Despite these benefits, the q-YSN suffers from large input current ripples, which call for a considerably larger input inductance and related power losses. The voltage gain of the existing MCIS networks can be generalized as $G = 1 / (1\text{-}K D_{ST})$, where K is a function of the windings turn ratio(s) and hence D_{ST} is theoretically limited by K as $0 < D_{ST} < 1/K$. Despite these benefits of the MCIS networks, a major challenge with these circuits is the leakage inductance, which decreases the effective shoot-through duration and voltage gain [37], and causes voltage spikes on the semiconductors and the dc-link [38, 39]. As a step forward, in order to improve the voltage gain characteristics of q-YSN, the diode-assisted Y-source network (DA-YSN) is recently introduced in [38], where 12 impedance source networks are proposed by basically integrating YSN, q-YSN, and DA-YSN with the quasi Z-source network [40] with the aim of tackling the voltage spikes across the dc-link. Due to the attractive advantage of the conventional YSN and q-YSN, they have been investigated from various points of view in the literature [37, 41–43]. However, in spite of the advantage of DA-YSN, the characteristics of this converter have not been adequately assessed.

DA-YSN offers a higher voltage gain than q-YSN with the same D_{ST} operation range and the same number of components. A considerably lower input current ripple is another attractive advantage of DA-YSN, which leads to a lower cost, size and losses of the input inductor. Furthermore, the magnetizing current ripple, the total voltage stress of the capacitors, and the total required capacitance of this network are all lower than YSN and q-YSN. Also, higher efficiency is attained due to the considerably lower total power loss of the magnetic element. In addition to the steady-state analysis, component design, and a thorough comparison with the state of the art, the circuit averaging method is used to model the nonlinear elements of the DA-YSN for the sake of dynamic studies. Finally, the validation of the theoretical achievements for DA-YSN is performed by extensive tests on a 200 W DC-DC converter prototype.

2 | CIRCUIT ANALYSIS

As shown in Figure 1a, DA-YSN introduces two additional windings to the circuit of the traditional single-switch quadratic boost converter in [44], and also uses an additional inductor and a diode in comparison to YSN of Figure 1b. Compared to the conventional q-YSN in Figure 1c, DA-YSN uses one less capacitor and one more diode. The diode assisted Γ-source network (DA-ΓSN) and diode assisted T-source network (DA-TSN) are also obtained from Figure 1a by removing the windings N_1 and N_2 from the original Y-shaped coupled inductor, respectively. The diode-assisted flipped-Γ-source network (DA-FΓSN) is also realized from DA-YSN by removing the winding N_3 and changing the dotted node of the winding N_2 of the coupled inductor. In what follows, DA-YSN is thoroughly investigated and the equations for the reduced versions can then be readily obtained by appropriate zero substituting for the removed winding of the original circuit.

2.1 | Operation principle

DA-YSN has the same operation states as other impedance source networks, that is, shoot-through (ST) and non-shoot-through (NST) states. The performance analysis is presented by assuming that the inductors operate in continuous conduction mode.

2.1.1 | Shoot-through state

Figure 2a shows the equivalent circuit of DA-YSN in ST state. During this state, the switch SW is ON, the diode D_1 is reverse-biased while the diode D_2 conducts, and the source and the capacitor C_1 charge the input and the coupled inductors, respectively. According to Figure 2a, for the voltage equations, one can write

$$\begin{cases} V_{Lin} = V_{in} \\ V_{N1} = \dfrac{N_1}{N_3 - N_2} V_{C1}. \end{cases} \tag{1}$$

It is worth mentioning that despite q-YSN, in all DA-ISNs, the voltage across the input inductance L_{in} during the ST state

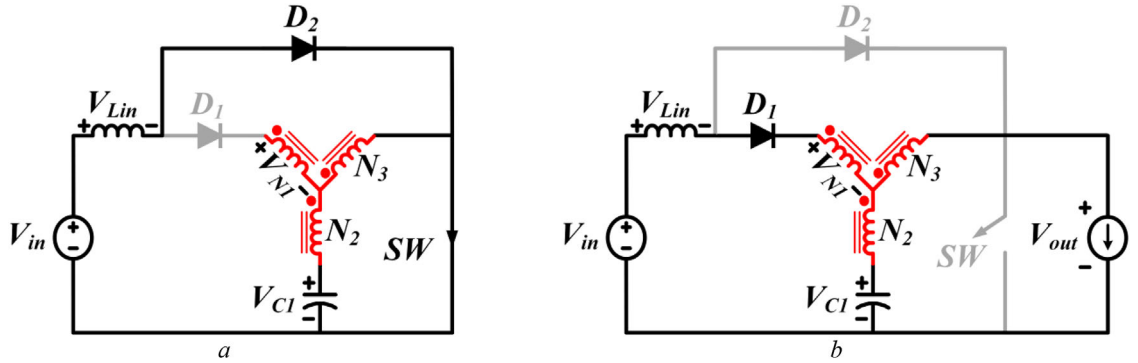

FIGURE 2 Equivalent circuits of DA-YSN. (a) ST state, (b) NST state

TABLE 1 Capacitor voltage and voltage gain of DA-ISNs

DA-ISNs	DA-YSN	DA-ΓSN	DA-TSN	DA-FΓSN
V_{C1}	$\frac{1}{1-\left(\frac{N_1+N_3}{N_3-N_2}\right)D_{ST}}V_{in}$	$\frac{1}{1-\left(\frac{N_3}{N_3-N_2}\right)D_{ST}}V_{in}$	$\frac{1}{1-\left(1+\frac{N_1}{N_3}\right)D_{ST}}V_{in}$	$\frac{1}{1-\frac{N_1}{N_2}D_{ST}}V_{in}$
Voltage gain (G)	$\frac{1}{1-D_{ST}}\times\frac{1}{1-\left(\frac{N_1+N_3}{N_3-N_2}\right)D_{ST}}$	$\frac{1}{1-D_{ST}}\times\frac{1}{1-\left(\frac{N_3}{N_3-N_2}\right)D_{ST}}$	$\frac{1}{1-D_{ST}}\times\frac{1}{1-\left(1+\frac{N_1}{N_3}\right)D_{ST}}$	$\frac{1}{1-D_{ST}}\times\frac{1}{1-\frac{N_1}{N_2}D_{ST}}$

is equal to the input voltage V_{in}. Therefore, the input current ripple is much lower than q-YSN.

2.1.2 | Non-shoot-through state

This state refers to the stage where the switch SW is turned off and D_1 conducts while D_2 blocks, as illustrated in Figure 2b. Moreover, the inductors and the source charge the capacitor C_1 and supply the load. The voltage equations are

$$V_{N1}=\frac{N_1}{N_1+N_2}(V_{in}-V_{C1}-V_{Lin}) \tag{2}$$

$$V_{out}=V_{in}-V_{Lin}-\left(1+\frac{N_3}{N_1}\right)V_{N1}. \tag{3}$$

In the steady-state, the average voltage across the inductor during a switching period is zero. Thus, the capacitor and the output voltages are obtained as (4).

$$\begin{cases} V_{C1}=\dfrac{1}{1-\delta D_{ST}}V_{in} \\ G=\dfrac{V_{out}}{V_{in}}=\dfrac{1}{1-D_{ST}}\times\dfrac{1}{1-\delta D_{ST}} \\ \delta=\dfrac{N_1+N_3}{N_3-N_2} \end{cases} \tag{4}$$

where δ is the winding factor. Following the same approach, the results for DA-ΓSN, DA-TSN and DA-FΓSN are obtained, and the results are summarized in Table 1.

For comparison purposes, the voltage gain of the conventional YSN and q-YSN and DA-YSN for different winding factors δ is reported in Table 2. Clearly, the boost ability of DA-YSN is higher than that of the two competitors, while the maximum value of the shoot-through duty cycle ($D_{ST,max}$) is the same for all networks. Also, in Table 2, the realization of the winding factor δ with different turn ratios is mentioned.

The winding factor for YSN and DA-YSN is equal to $\delta=\frac{N_1+N_3}{N_3-N_2}$ while for q-YSN, it is $\delta=\frac{N_1+N_2}{N_2-N_3}$. Due to a positive δ, for YSN and DA-YSN $N_3>N_2$ and for q-YSN $N_2>N_3$. Consequently, the same coupled inductor leads to the same δ for all converters by interchanging the windings N_2 and N_3 in q-YSN in comparison to YSN and DA-YSN. The voltage gains of YSN, q-YSN and DA-YSN versus D_{ST} are plotted in Figure 3a for various δ. It is notable that for the same voltage gain, the ST period for DA-YSN is shorter than the competitors. The enhanced boost ability of the networks makes them suitable for distributed power generation applications, where a high gain is often demanded. The plotted voltage gains of Y-shaped networks in Figure 3a are calculated under an ideal lossless condition. However, the practical voltage gain is seriously affected by the parasitic elements, including the equivalent series resistance (ESR) of the inductors and capacitors, ON-state resistance of the diodes and the switch, and the voltage drop of the diodes. According to a procedure detailed in [42], the non-ideal voltage gain of the Y-shaped networks are calculated based

TABLE 2 Voltage gain comparison and turn numbers realization for various winding factors

δ	Voltage gain		$D_{ST,max}$	N_1:N_2:N_3	
	YSN & q-YSN	DA-YSN		YSN & DA-YSN	q-YSN
2	$\frac{1}{1-2D_{ST}}$	$\frac{1}{1-D_{ST}} \times \frac{1}{1-2D_{ST}}$	0.5	(1:1:3), (2:1:4), (3:1:5)	(1:3:1), (2:4:1), (3:5:1)
3	$\frac{1}{1-3D_{ST}}$	$\frac{1}{1-D_{ST}} \times \frac{1}{1-3D_{ST}}$	0.33	(1:1:2), (3:1:3), (1:3:5)	(1:2:1), (3:3:1), (1:5:3)
4	$\frac{1}{1-4D_{ST}}$	$\frac{1}{1-D_{ST}} \times \frac{1}{1-4D_{ST}}$	0.25	(2:1:2), (1:2:3), (5:1:3)	(2:2:1), (1:3:2), (5:3:1)
5	$\frac{1}{1-5D_{ST}}$	$\frac{1}{1-D_{ST}} \times \frac{1}{1-5D_{ST}}$	0.2	(1:3:4), (3:1:2), (2:2:3)	(1:4:3), (3:2:1), (2:3:2)
6	$\frac{1}{1-6D_{ST}}$	$\frac{1}{1-D_{ST}} \times \frac{1}{1-6D_{ST}}$	0.17	(4:1:2), (3:2:3), (2:3:4)	(4:2:1), (3:3:2), (2:4:3)

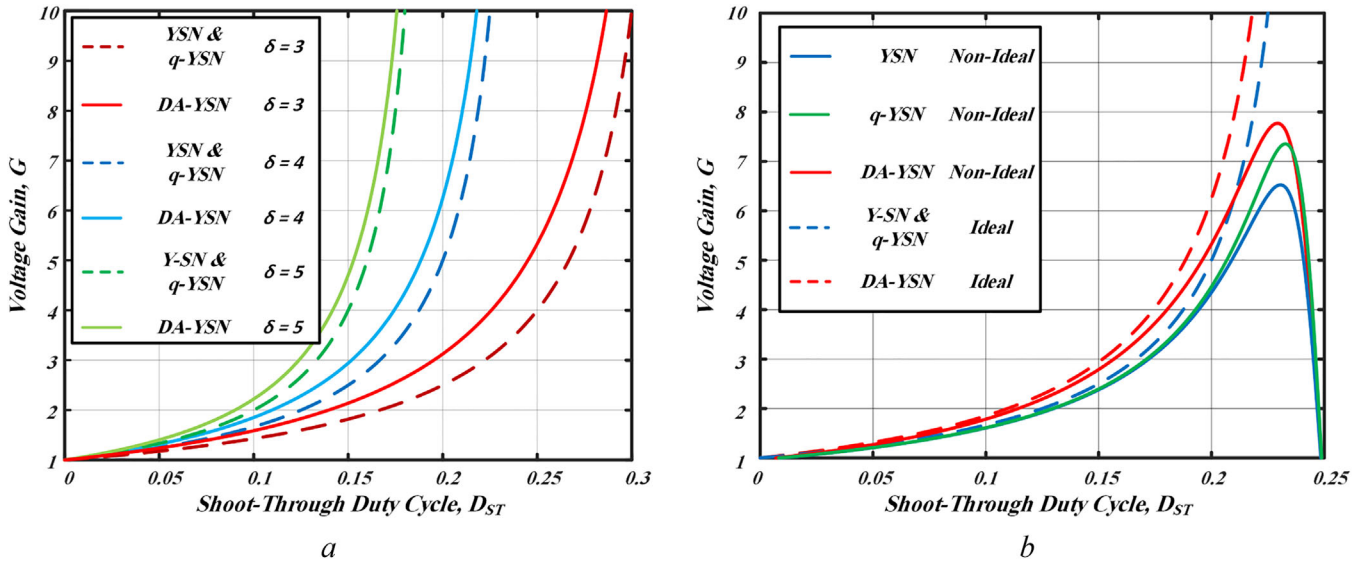

FIGURE 3 Voltage gain comparison of Y-shaped networks. (a) Ideal lossless and (b) Ideal and non-ideal ($\delta = 4$) conditions

on the experimental conditions (refer to Table 8) and $\delta = 4$, and the results are plotted in Figure 3b. As already expected, the voltage gain under non-ideal condition is lower than the ideal lossless condition. Also, as shown in Figure 3b, the voltage gain can theoretically change from one to infinite under the ideal lossless condition while it is seriously limited when considering the parasitic elements. It is notable that under the non-ideal condition, the voltage gain increases with the increase of D_{ST} first, and then decreases after reaching a peak value. After all, one can conclude from this study that DA-YSN offers higher voltage gain under both ideal and non-ideal conditions.

3 | COMPONENT DESIGN

The major part of any impedance network, which mainly determines its volume and cost, is the passive components. In this section, a straightforward design procedure to decide the values of the input and magnetizing inductances and the capacitor, considering different practical and theoretical constraints, is presented.

3.1 | Input inductance (L_{in})

The input inductance (L_{in}) is designed based on its voltage (V_{Lin}), dwell time of the corresponding state of operation (Δt) and the input current ripple (Δi_{in}) as

$$L_{in} = V_{Lin} \frac{\Delta t}{\Delta i_{in}}. \tag{5}$$

Thus, the input inductance of DA-YSN can be designed as

$$L_{in} = D_{ST} \times L_{in}^{Base} \tag{6}$$

where

$$L_{in}^{Base} = \frac{V_{in}^2 T_s}{\alpha\% P} \tag{7}$$

with P as the rated power, T_s as the switching period, and considering α % of the input current as its maximum ripple.

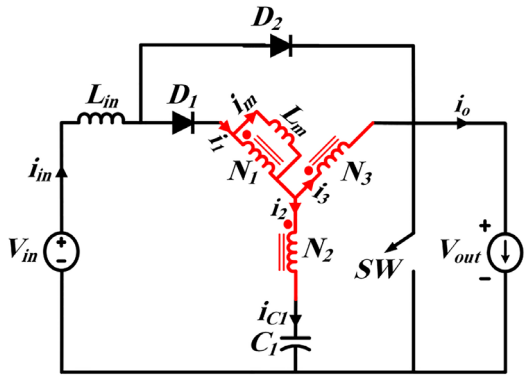

FIGURE 4 DA-YSN by considering the magnetizing inductance

3.2 | Magnetizing inductance (L_m)

The magnetizing inductance can be designed by using the similar approach followed for the input inductance. Thus, with $\beta\%$ as the maximum tolerable magnetizing current ripple, the magnetizing inductance can be obtained as

$$L_m = \frac{N_1^2}{(N_3 - N_2)(N_1 + N_3)} \times D_{ST}\, G \times L_m^{Base} \tag{8}$$

where L_m is the magnetizing inductance when referred to the winding N_1, as shown in Figure 4, and L_m^{Base} is

$$L_m^{Base} = \frac{V_{in}^2 T_s}{\beta\% P}. \tag{9}$$

3.3 | Capacitances

The capacitance is designed based on the charge current through it and the time duration, as

$$C = \frac{I_C}{\Delta V_C}\Delta t \tag{10}$$

where ΔV_C is the capacitor voltage ripple. Thus, the capacitance of DA-YSN can be designed by assuming $\gamma\%$ of the capacitor voltage as its ripple, as

$$C_1 = \left(\frac{1}{G} - \frac{1}{G^2(1 - D_{ST})}\right) \times C_{Base} \tag{11}$$

where

$$C_{Base} = \frac{P T_s}{\gamma\% V_{in}^2}. \tag{12}$$

4 | NETWORKS COMPARISON

To clarify the superiority of the diode-assisted Y-source network over the other MCIS networks, this section compares DA-YSN to successful competitors. The results are summarized in Table 3. Besides the average and ripple of the magnetizing current, the input current ripple, the capacitor voltage stress, the total capacitance, the winding volume, copper losses and the total volume of the passive components of DA-YSN are compared to those of YSN and q-YSN.

4.1 | Magnetizing current

For a three-winding coupled inductor, the magnetizing current is determined from (13).

$$N_1 i_1 + N_2 i_2 + N_3 i_3 = N_1 i_m \tag{13}$$

where i_1, i_2 and i_3 are the windings' current and i_m is the magnetizing current referred to the winding N_1, which is shown in Figure 4. In ST state, the capacitor current is

$$I_{C1}^{ST} = -\frac{N_1}{N_3 - N_2} I_m^{ST} \tag{14}$$

where I_m^{ST} is the average of the magnetizing current (referred to N_1) in ST state.

For NST state, by considering I_o^{NST} and I_{in}^{NST} as the average of the output and input currents in this state, one can write

$$I_{C1}^{NST} = I_{in}^{NST} - I_o^{NST}. \tag{15}$$

By applying the capacitor charge balance principle to the capacitor current of (14) and (15), the average of the magnetizing current is derived as

$$I_m = (1 - D_{ST})\left(1 + \frac{N_3}{N_1}\right) I_{in}. \tag{16}$$

For YSN, the average of the magnetizing current is calculated as

$$I_m = \left(1 + \frac{N_3}{N_1}\right) I_{in}. \tag{17}$$

From (16) and (17), it is obvious that the average magnetizing current of DA-YSN is lower than that of conventional YSN. Also, the average magnetizing current of q-YSN is zero, which is the lowest.

To calculate the magnetizing current ripple, as given in (18), the voltage across the winding N_1 and its time duration are required.

$$\Delta i_m = \frac{V_{N1}\,\Delta t}{L_m}. \tag{18}$$

Thus, for DA-YSN, one can write

$$\Delta i_m = \frac{N_1}{N_3 - N_2} \frac{(1 - D_{ST})\, G\, V_{in}\, D_{ST}\, T_s}{L_m}. \tag{19}$$

TABLE 3 Comparison of Y-shaped networks

Converter	δ	Voltage gain (G)	V_{Ctotal}/V_{out}	V_{Dtotal}/V_{out} I_{Dtotal}/I_{in}	I_{SW}^{ST}/I_{in}	I_m/I_{in}	$\Delta i_{in}/\Delta i_{in}^{Base}$
DA-YSN [38]	$\frac{N_1+N_3}{N_3-N_2}$	$\frac{1}{1-D_{ST}}\times\frac{1}{1-\delta D_{ST}}$	$1-D_{ST}$	$\delta 2$	$\frac{1-\frac{1}{(1-D_{ST})G}}{D_{ST}}$	$(1-D_{ST})\left(1+\frac{N_3}{N_1}\right)$	D_{ST}
YSN [28]	$\frac{N_1+N_3}{N_3-N_2}$	$\frac{1}{1-\delta D_{ST}}$	$1-D_{ST}$	$\delta-1\frac{1}{1-D_{ST}}$	$\frac{1-\frac{1}{(1-D_{ST})G}}{D_{ST}}$	$1+\frac{N_3}{N_1}$	—
q-YSN [32]	$\frac{N_1+N_2}{N_2-N_3}$	$\frac{1}{1-\delta D_{ST}}$	$1+(\delta-2)D_{ST}$	$\frac{1}{1-D_{ST}}$	$\frac{1-\frac{1}{(1-D_{ST})G}}{D_{ST}}$	0	$(1-D_{ST})(G-1)$

*$\Delta i_{in}^{Base}=V_{in}T_s/L_{in}$.

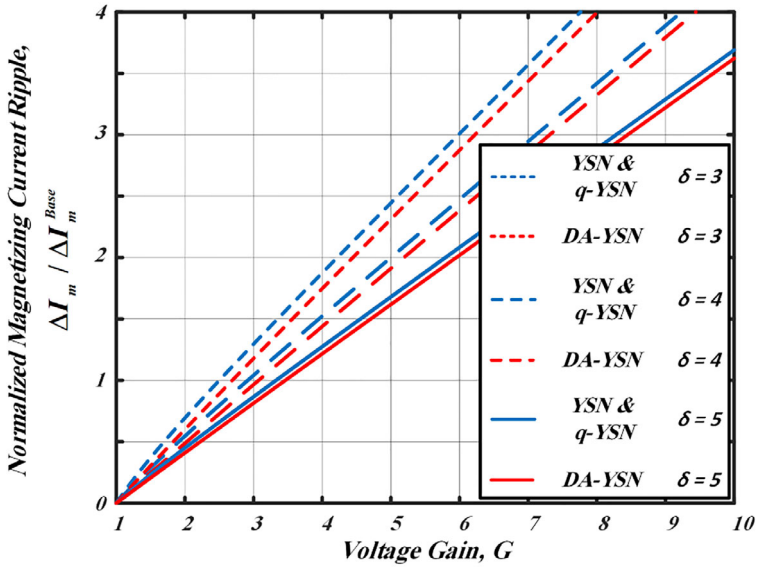

FIGURE 5 Magnetizing current ripple comparison

In Figure 5, the magnetizing current ripples of the three Y-shaped networks are plotted by considering the same δ. From this figure, the magnetizing current ripple of DA-YSN is lower than those of the conventional YSN and q-YSN, which leads to a lower core loss [45]. The normalizing factor in this figure is

$$\Delta I_m^{Base}=\frac{V_{in}T_s}{L_m}. \tag{20}$$

4.2 | Input current ripple

The improved input current profile is one of the advantages of DA-YSN and q-YSN over YSN. Figure 6a compares the normalized input current ripple of DA-YSN and q-YSN for various δ, where ΔI_{in}^{Base} is

$$\Delta I_{in}^{Base}=\frac{V_{in}T_s}{L_{in}}. \tag{21}$$

Clearly, the input current ripple of DA-YSN is considerably lower than that of q-YSN, which leads to a lower core loss and also makes it a suitable choice for renewable energy systems. It is notable that for DA-YSN, by increasing the winding factor in order to increase the voltage gain, the normalized input current ripple decreases while the opposite occurs for q-YSN.

4.3 | Total voltage stress on capacitors

The capacitor voltage stress of DA-YSN is calculated based on (4). Also, the total voltage stress of other networks is obtained from Table 3. For a better comparison between the Y-shaped networks, in Figure 6b, the total voltage stress on capacitors is plotted, assuming the same input voltage. As shown in this figure, the total voltage stress for DA-YSN and YSN is almost the same and considerably lower than that of q-YSN.

4.4 | Total capacitances

The normalized total capacitances required for DA-YSN, YSN and q-YSN are shown in Figure 6c, in which C_{Base} is defined as (12). As shown in this figure, the required capacitance of DA-

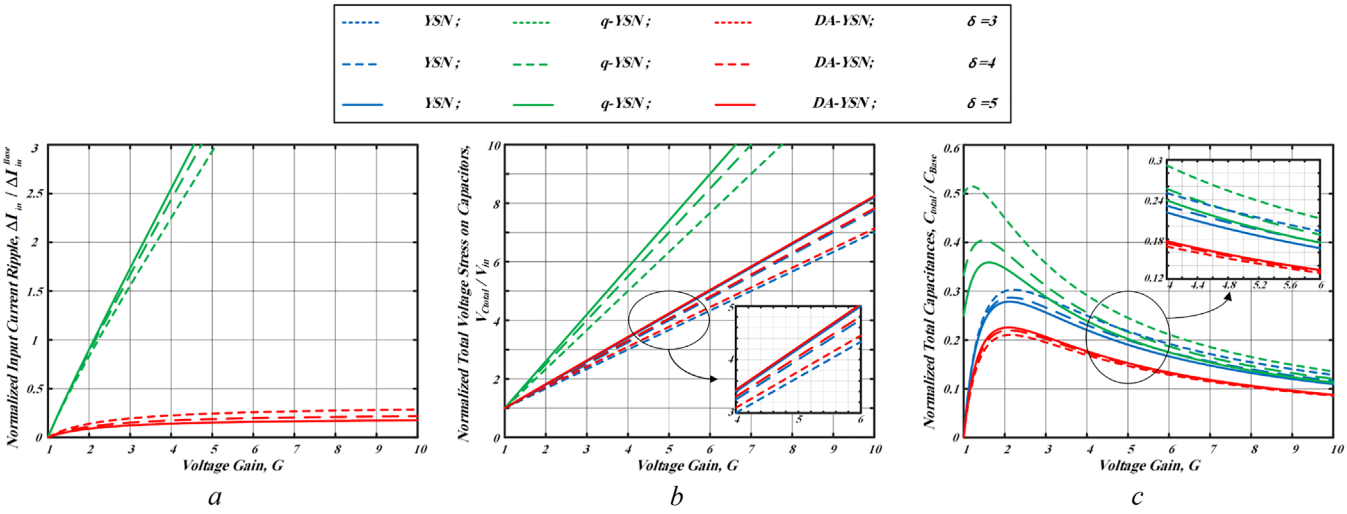

FIGURE 6 Comparison of DA-YSN with competitors. (a) Input current ripple, (b) Total voltage stress on capacitors, (c) Total required capacitances

TABLE 4 Copper loss and windings volume comparison

Converter	$i_{1,rms}$ (N_1)	$i_{2,rms}$ (N_2)	$i_{3,rms}$ (N_3)	$\sum N_j i^2_{j,rms}$	$\sum N_j i_{j,rms}$
DA-YSN	3.60 (120)	6.44 (24)	5.95 (72)	5100	1015
YSN	4.15 (120)	8.05 (24)	7.15 (72)	7303	1206
q-YSN	2.34 (120)	7.22 (72)	9.52 (24)	6585	1029

YSN is the lowest. Also, because of the use of an additional capacitor, the total required capacitances of q-YSN is higher than YSN.

4.5 | Total volume and power losses of the coupled inductor windings

As other important practical parameters, the winding loss and volume (weight) are compared in Table 4 for experimental conditions, as done in [30]. In this table, the sum of $N_j i^2_{j,rms}$ reflects the copper loss, while the sum of $N_j i_{j,rms}$ is proportionally related to the winding volume (weight). Consequently, the winding copper loss of DA-YSN is lower than YSN and q-YSN by 30.2% and 22.5%, respectively. Also, for DA-YSN, the winding volume or weight is lower than YSN and q-YSN by 15.8% and 1.4%, respectively.

4.6 | Total volume of the passive components

Two parameters determine the inductors' volume: maximum stored energy and fill factor (K_u). According to [45], the first one can be attained as

$$W^{\max}_{core} \propto L_m I^2_{m,\max} \tag{22}$$

where L_m can be obtained from (19), and $I_{m,max}$ is the peak magnetizing current. By taking the experimental parameters in Table 8 into account, the required magnetizing inductance is 952 μH for YSN and q-YSN, and 900 μH for DA-YSN to obtain the same $\Delta i_m = 3.2$ A for three Y-shaped networks. Also, the input inductor, L_{in} is considered as 2437 μH for q-YSN and 175 μH for DA-YSN to have the same input current ripple ($\alpha = 50\%$). Therefore, the first parameter for the magnetic core selection, that is, the maximum stored energy, is calculated for all understudy cases while Table 5 shows the consequences. When the first core with a higher $LI_{m,max}{}^2$ than the calculated value is chosen, it never will be saturated [46]. Next, according to the fraction of the current density (J) and the RMS value of the windings current (I_{rms}), the wire bare area (A_{wire}) of each winding should be specified as $A_{wire} = I_{rms}/J$. Often, J is selected between 3 and 8 A/mm^2 while the wire length and efficiency improvement are supposed. Therefore, the current density is selected as 4 A/mm^2 here, for all impedance source networks. Eventually, the litz wire is utilized in order to reduce the AC resistance of windings and cover the required A_{wire}. As the second parameter for core selection K_u is defined as the proportion of the total conductor cross-section to the area of the core window and usually is selected below 65% [46]. Accordingly, the proper magnetic cores are chosen for all Y-shaped networks while the results are presented in Table 5. Furthermore, the volume of the cores is reported in this table. Based on Table 5, the sum of the

TABLE 5 Numerical design of the inductors of Y-shaped networks

Conv.	Ind.	L (μH)	L $(I_{Lmax})^2$ (mH A^2)	Part num. of core	Volume Par.	Volume mm^3	Turn	K_u (%)	MLT (mm)
YSN	L_m	952	60.93	0077620A7	Core	51800	70:14:42	23	93
					Win.	18488			
q-YSN	L_m	952	2.43	0077585A7	Core	4150	125:75:25	63	52
					Win.	14040			
	L_{in}	2437	60.92	0077617A7	Core	51800	131	16.2	90
					Win.	11790			
DA-YSN	L_m	900	42.65	0077195A7	Core	28600	80:16:48	32	75
					Win.	13680			
	L_{in}	175	4.37	0077586A7	Core	4150	77	18.5	38

TABLE 6 Numerical design of capacitors of the Y-shaped networks

Conv.	Cap.	Capacitance (μF)	Capacitor voltage (V)	CV_{max}^2 (mF V^2)
YSN	C_1	30	162.5	808.11
	C_o	1.87	200	76.30
	Total	31.87	362.5	884.41
q-YSN	C_1	30	162.5	808.11
	C_2	13.33	123	205.72
	C_o	1.87	200	76.30
	Total	45.2	485.5	1090.13
DA-YSN	C_1	27.88	165	774.29
	C_o	1.74	200	71
	Total	29.62	365	845.29

magnetizing and input inductors core size is 51,800 mm^3, 55,950 mm^3 and 32,750 mm^3 for YSN, q-YSN and DA-YSN, respectively. As a result, YSN and q-YSN are 1.6 and 1.7 times bulkier than DA-YSN when the magnetic components are under investigation parameters.

Similar to the inductors, maximum stored energy ($C\,V^2_{max}$) determines the volume of the capacitors. To compare the capacitor volume, the capacitors are numerically designed for Y-shaped networks to achieve 2% voltage ripple and the results are summarized in Table 6. Also, the total CV^2_{max} is calculated for all networks in this table. Therefore, YSN and q-YSN are 1.05 and 1.29 times bulkier than DA-YSN in terms of the capacitors.

Generally, one can conclude that DA-YSN with the high step-up capability offers high power density due to the lower reactive element requirement in comparison to competitors.

5 | SMALL-SIGNAL MODEL

The small-signal model is used to approximate the behavior of power electronic converters with linear equations, which provides a means for dynamic and control studies. For this purpose,

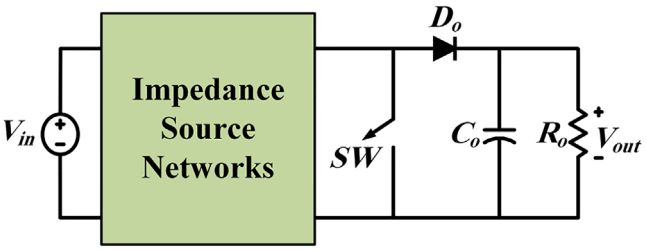

FIGURE 7 Impedance source networks for DC-DC application

the nonlinear elements of the impedance source networks, that is, diodes and switches, are modelled as dependent voltage or current sources [34]. For the sake of simplicity, and in accordance to the experimental setup, the small-signal models are presented for DC-DC power conversion, as shown in Figure 7.

The circuit averaging technique involves averaging the current and the voltage of nonlinear elements during a switching period. The average of the diodes' voltage ($\bar{V}_D$) and the switch current ($\bar{I}_{SW}$) of DA-YSN can be obtained from (23) and (24), respectively.

$$\begin{cases} \bar{V}_{D1} = \bar{V}_{D2} = \delta \times D_{ST} \times (1 - D_{ST}) \times G \times V_{in} \\ \bar{V}_{Do} = G \times D_{ST} \times V_{in} \end{cases} \tag{23}$$

$$\bar{I}_{SW} = \left(1 - \frac{1}{G}\right) \times I_{in} \tag{24}$$

where δ can be calculated from (4). Considering the values with a $\sim$ as small-signal perturbations around the operation point and replacing G from (4), the large-signal equations can be obtained as

$$\begin{cases} \bar{V}_{D1,2} + \tilde{v}_{D1,2} = \dfrac{\delta \times (D_{ST} + \tilde{d}_{ST})}{1 - \delta \times (D_{ST} + \tilde{d}_{ST})} \times (V_{in} + \tilde{v}_{in}) \\ \bar{V}_{Do} + \tilde{v}_{Do} = \dfrac{1}{1 - (D_{ST} + \tilde{d}_{ST})} \times \dfrac{(D_{ST} + \tilde{d}_{ST})}{1 - \delta \times (D_{ST} + \tilde{d}_{ST})} \\ \qquad \times (V_{in} + \tilde{v}_{in}) \end{cases} \tag{25}$$

TABLE 7 Small-signal coefficients for reduced versions of DA-ISNs

Networks	DA-ΓSN	DA-TSN	DA-FΓSN
α_1	$\frac{\frac{N_3}{N_3-N_2}\times D_{ST}}{1-\frac{N_3}{N_3-N_2}\times D_{ST}}$	$\frac{\frac{N_1+N_3}{N_3}\times D_{ST}}{1-\frac{N_1+N_3}{N_3}\times D_{ST}}$	$\frac{\frac{N_1}{N_2}\times D_{ST}}{1-\frac{N_1}{N_2}\times D_{ST}}$
α_2	$\frac{1}{1-D_{ST}}\times\frac{D_{ST}}{1-\frac{N_3}{N_3-N_2}\times D_{ST}}$	$\frac{1}{1-D_{ST}}\times\frac{D_{ST}}{1-\frac{N_1+N_3}{N_3}\times D_{ST}}$	$\frac{1}{1-D_{ST}}\times\frac{D_{ST}}{1-\frac{N_1}{N_2}\times D_{ST}}$
α_3	$\left(1+\frac{N_3}{N_3-N_2}(1-D_{ST})\right)\times D_{ST}$	$\left(1+\frac{N_1+N_3}{N_3}(1-D_{ST})\right)\times D_{ST}$	$\left(1+\frac{N_1}{N_2}(1-D_{ST})\right)\times D_{ST}$
β_1	$\frac{\frac{N_3}{N_3-N_2}\times V_{in}}{(1-\frac{N_3}{N_3-N_2}\times D_{ST})^2}$	$\frac{\frac{N_1+N_3}{N_3}\times V_{in}}{(1-\frac{N_1+N_3}{N_3}\times D_{ST})^2}$	$\frac{\frac{N_1}{N_2}\times V_{in}}{(1-\frac{N_1}{N_2}\times D_{ST})^2}$
β_2	$\frac{V_{in}}{(1-D_{ST})^2}\times\frac{1-\frac{N_3}{N_3-N_2}\times D_{ST}^2}{(1-\frac{N_3}{N_3-N_2}\times D_{ST})^2}$	$\frac{V_{in}}{(1-D_{ST})^2}\times\frac{1-\frac{N_1+N_3}{N_3}\times D_{ST}^2}{(1-\frac{N_1+N_3}{N_3}\times D_{ST})^2}$	$\frac{V_{in}}{(1-D_{ST})^2}\times\frac{1-\frac{N_1}{N_2}\times D_{ST}^2}{(1-\frac{N_1}{N_2}\times D_{ST})^2}$
β_3	$\left[\frac{N_3}{N_3-N_2}(1-2D_{ST})+1\right]\times I_{in}$	$\left[\frac{N_1+N_3}{N_3}(1-2D_{ST})+1\right]\times I_{in}$	$\left[\frac{N_1}{N_2}(1-2D_{ST})+1\right]\times I_{in}$

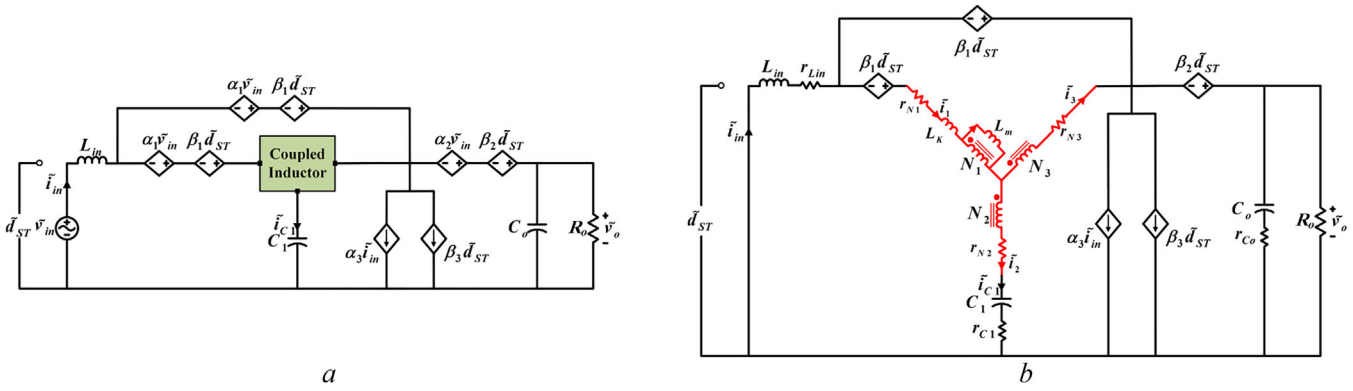

FIGURE 8 Small-signal models. (a) DA-ISNs, (b) DA-YSN

$$\bar{I}_{SW}+\tilde{i}_{SW}=[(\delta+1)\times(D_{ST}+\tilde{d}_{ST})-\delta\times(D_{ST}+\tilde{d}_{ST})^2]\times(I_{in}+\tilde{i}_{in}). \tag{26}$$

The dynamic (small-signal) part of (25) and (26) can be extracted as

$$\begin{cases}\tilde{v}_{D1,2}=\dfrac{\delta\times D_{ST}}{1-\delta\times D_{ST}}\tilde{v}_{in}+\dfrac{\delta\times V_{in}}{(1-\delta\times D_{ST})^2}\tilde{d}_{ST}\\ \tilde{v}_{Do}=\dfrac{1}{1-D_{ST}}\times\dfrac{D_{ST}}{1-\delta\times D_{ST}}\tilde{v}_{in}+\dfrac{1-\delta\times D_{ST}^2}{(1-D_{ST})^2}\\ \qquad\times\dfrac{V_{in}}{(1-\delta\times D_{ST})^2}\tilde{d}_{ST}\end{cases} \tag{27}$$

$$\tilde{i}_{SW}=(\delta(1-D_{ST})+1)\times D_{ST}\times\tilde{i}_{in}+(\delta+1-2\delta D_{ST})\times I_{in}\times\tilde{d}_{ST} \tag{28}$$

or

$$\begin{cases}\tilde{v}_{D1}=\tilde{v}_{D2}=\alpha_1\tilde{v}_{in}+\beta_1\tilde{d}_{ST}\\ \tilde{v}_{Do}=\alpha_2\tilde{v}_{in}+\beta_2\tilde{d}_{ST}\\ \tilde{i}_{SW}=\alpha_3\tilde{i}_{in}+\beta_3\tilde{d}_{ST}.\end{cases} \tag{29}$$

Using the same approach, the small-signal coefficients (α and β) for the reduced versions of DA-ISNs are calculated and given in Table 7. The diodes and the switch are replaced by the controlled voltage and current sources, respectively, as shown in Figure 8a. The coupled inductor block in the model can be replaced by the Y, Γ, T and flipped Γ shaped coupled inductors. This model can be used for dynamic studies, and the obtained transfer functions of this model facilitate controller design and closed-loop performance analysis according to the desired application requirements. Any required transfer function can be readily obtained from this model. Accordingly, the control-to-output transfer function for DA-YSN can be calculated from the model of Figure 8b, which is derived from

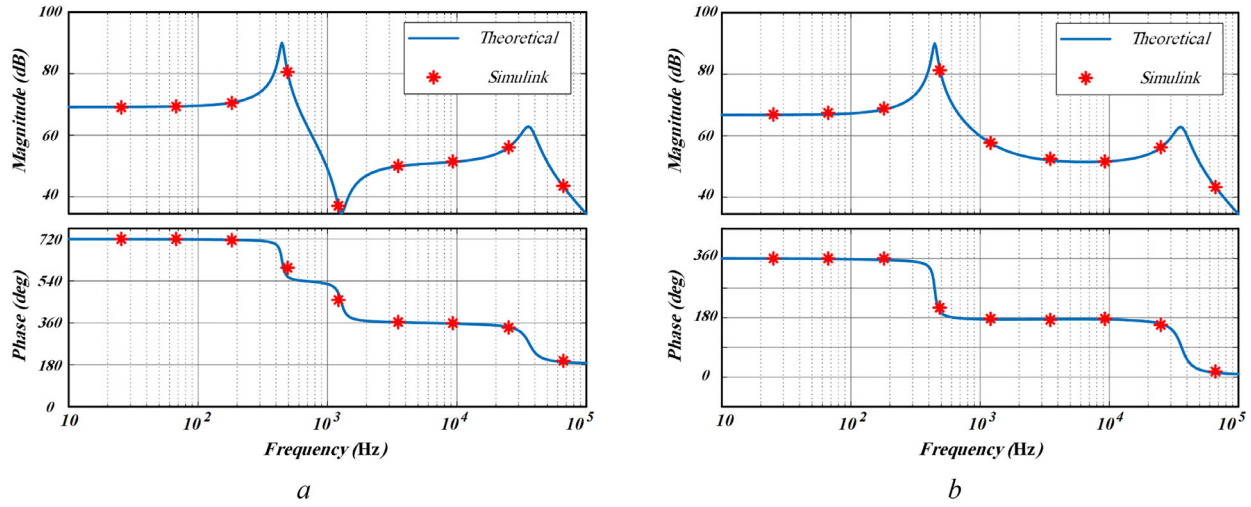

FIGURE 9 Bode plots of DA-YSN transfer functions. (a) Control-to-output voltage and (b) Control-to-capacitor voltage

Figure 8a by replacing the coupled inductor block with the Y-shaped coupled inductor and neglecting the perturbation of the input voltage, $\tilde{v}_{in}$, that is, $\tilde{v}_{in} = 0$. In this model, the equivalent series resistance (ESR) of passive components are considered, as shown in Figure 8b. Also, L_K represents the total leakage inductance transferred to the winding N_1 of the coupled inductor.

The control-to-output/capacitor voltage transfer functions can be obtained by writing some KVLs and KCLs in the S-domain for the circuit of Figure 8b.

$$\begin{cases} KCL_1 : \tilde{i}_{C1} = (1-\alpha_3)\tilde{i}_{in} - \beta_3\,\tilde{d}_{ST} - \dfrac{\tilde{v}_{out}}{Z_o} \\ KCL_2 : \tilde{i}_1 - \tilde{i}_3 = \tilde{i}_2 = \tilde{i}_{C1} \\ KVL_1 : (r_{N1} + Z_K)\tilde{i}_1 + \left(1 + \dfrac{N_3}{N_1}\right) Z_m \tilde{i}_m + r_{N1}\tilde{i}_3 = 0 \\ KVL_2 : Z_{Lin}\tilde{i}_{in} - \beta_1\,\tilde{d}_{ST} - \beta_2\,\tilde{d}_{ST} + \tilde{v}_{out} = 0 \end{cases} \tag{30}$$

where

$$\begin{cases} Z_o = \left(\dfrac{1}{s\,C_o} + r_{Co}\right) || R_o,\ Z_{Lin} = s\,L_{in} + r_{Lin} \\ Z_m = s\,L_m,\ \ Z_K = s\,L_K. \end{cases} \tag{31}$$

From (13), the magnetizing current (referred to N_1) can be calculated as

$$\tilde{i}_m = \tilde{i}_1 + \frac{N_2}{N_1}\tilde{i}_2 + \frac{N_3}{N_1}\tilde{i}_3. \tag{32}$$

By applying KVL to the loop including capacitor C_1, coupled inductor windings N_2 and N_3, output diode, and load, one yields

$$\tilde{v}_{out} = (Z_{C1} + r_{N2})\tilde{i}_{C1} - \frac{N_3 - N_2}{N_1} Z_m \tilde{i}_m - r_{N3}\tilde{i}_3 + \beta_2\,\tilde{d}_{ST} \tag{33}$$

TABLE 8 Experimental setup parameters

Parameter	Value
Input voltage, V_{in}	50 V
Output voltage, V_o	200 V
Rated power, P	200 W
Switching frequency	25 kHz
Magnetic core	0077615A7
Magnetizing inductor, L_m	1.2 mH
Winding turns	120:24:72
Leakage inductance, ESRL_{K1}, r_{N1}	13.6 μH, 0.19 Ω
L_{K2}, r_{N2}	1.23 μH, 0.05 Ω
L_{K3}, r_{N3}	0.6 μH, 0.12 Ω
Capacitors, $C_{1,o}$	16 μF (5 mΩ)
C_2	48 μF (11 mΩ)
Input inductor, L_{in}	1 mH (60 mΩ)
Diodes, D_1 & $D_{2,o}$	RHRG75120 & APT30D60B
Switch, SW	SPW47N60CFD

where

$$Z_{C1} = \left(\frac{1}{s\,C_1} + r_{C1}\right). \tag{34}$$

Finally, by solving (30)–(32) for $\tilde{i}_1$, $\tilde{i}_2$, $\tilde{i}_3$, $\tilde{i}_m$ and $\tilde{i}_{in}$, and substituting them in (33), the control-to-output transfer function of DA-YSN can be calculated. Also, the control-to-capacitor voltage transfer function can be obtained from (30)–(34) and $\tilde{v}_{C1} = Z_{C1}\tilde{i}_{C1}$.

These transfer functions are calculated with the experimental setup parameters (refer to Table 8), and the results are given in (35). The Bode plots of the transfer functions calculated in (35) are shown in Figure 9. Also, in order to confirm the validity of

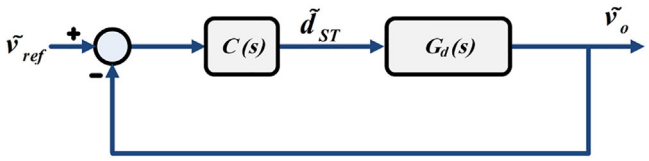

FIGURE 10 Voltage loop control scheme of DA-YSN

the derived transfer functions, the linear small-signal model of DA-YSN was implemented in Simulink software. In Figure 9, the simulation and calculation Bode plots are compared. As all effective parasitic parameters are considered in both calculation and simulation studies, the Bode plots are almost similar, which confirms the derived transfer functions.

DA-YSN adopts an output voltage control loop, shown in Figure 10, where $G_d(s)$ is the control-to-output transfer function and $C(s)$ is the proportional-integral (PI) controller transfer function of (36).

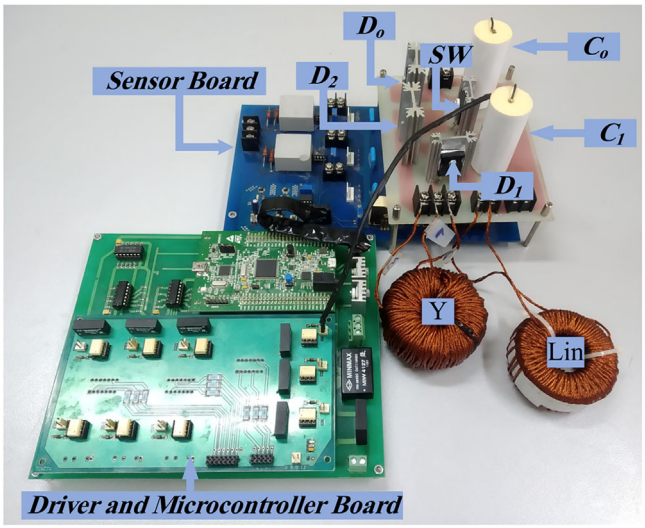

FIGURE 11 Experimental prototype

$$\begin{cases} G_{vo-d}(s) = \dfrac{\tilde{v}_{out}}{\tilde{d}_{ST}} = \dfrac{-0.07\,s^5 + 5.53\times10^5\,s^4 + 1.82\times10^{13}\,s^3 - 1.78\times10^{16}\,s^2 + 1.16\times10^{21}\,s + 1.18\times10^{23}}{s^5 + 5.82\times10^4\,s^4 + 5.18\times10^{10}\,s^3 + 1.73\times10^{13}\,s^2 + 4.06\times10^{17}\,s + 4.11\times10^{19}} \\ G_{vc-d}(s) = \dfrac{\tilde{v}_{C1}}{\tilde{d}_{ST}} = \dfrac{-1.45\times10^6\,s^4 - 1.82\times10^{13}\,s^3 - 3.18\times10^{16}\,s^2 + 8.77\times10^{20}\,s + 8.94\times10^{22}}{s^5 + 5.82\times10^4\,s^4 + 5.18\times10^{10}\,s^3 + 1.73\times10^{13}\,s^2 + 4.06\times10^{17}\,s + 4.11\times10^{19}}. \end{cases} \tag{35}$$

$$C(s) = K_P + \frac{K_I}{s} \tag{36}$$

A frequency-domain design approach presented in [47] is employed here, which results in $K_P = 1.535\times10^{-6}$ and $K_I = 0.031$. The closed-loop system is stable with zero overshoot, and the rise and settling times in response to a step-change in the reference are almost 25 ms and 43 ms, respectively.

6 | EXPERIMENTAL RESULTS

A DC-DC converter shown in Figure 7 is implemented, which includes an additional capacitor C_o, diode D_o and load resistor R_o. A photo of the experimental setup is shown in Figure 11, and the experimental parameters are summarized in Table 8. For the sake of a fair comparison, the same passive and active components are chosen for all under-test converters. For YSN and DA-YSN, the turn ratios are chosen as 5:1:3 and for q-YSN, as 5:3:1, which translates to the same winding factor as $\delta = 4$ for all converters. According to Table 2, the shoot-through duty cycle D_{ST} for YSN and q-YSN is obtained as 0.1875, while for DA-YSN is 0.1743 to achieve the desired voltage gain of $G = 4$. It should be noted that the magnetic element is realized on a toroidal magnetic core with KoolMμ® material from Magnetics®, which offers a considerably low core loss profile. Moreover, the coupled inductors are constructed from multistrand Litz wires with the interleaved winding method that simultaneously let a lower copper loss and reduced leakage inductances.

Figures 12–14 are the experimental waveforms of DA-YSN, YSN and q-YSN, respectively. The input and output voltages and currents are presented in Figures 12–14a. Obviously, unlike conventional YSN, the input current of q-YSN and DA-YSN is continuous. Also, the input current ripple of DA-YSN is considerably lower than q-YSN. Thus, the very low input current ripple of DA-YSN and its high voltage gain is best fitted to renewable and distributed power generation applications. Also, the output voltage of DA-YSN is the highest, that indicates a better regulation (lower voltage drop) of this converter when considering the same components, as expected from Figure 3b. The output voltages of DA-YSN, YSN and q-YSN are calculated theoretically (under ideal and non-ideal conditions from Figure 3), and also calculated from PSIM thermal module simulation, and the results are summarized in Table 9 along with the experimental ones read from Figures 12–14a. A better voltage regulation of DA-YSN can be concluded from Table 9 in terms of a better match of simulation and experimental results with the theoretical one. In addition, Figures 12–14b from top to bottom show the measured input, output and capacitor voltages of the understudy networks, respectively. The measured amplitudes are in good agreement with the theoretical equations in Section 2.

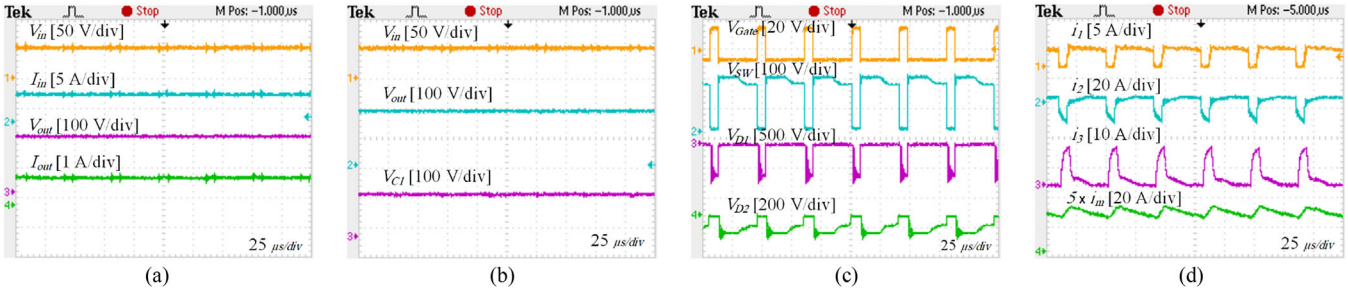

FIGURE 12 DA-YSN experimental results. (a) Input and output voltages and currents, (b) Input, output and capacitor C_1 voltages, (c) ST pulses and blocking voltages of active elements, (d) Windings N_1 to N_3 and magnetizing currents

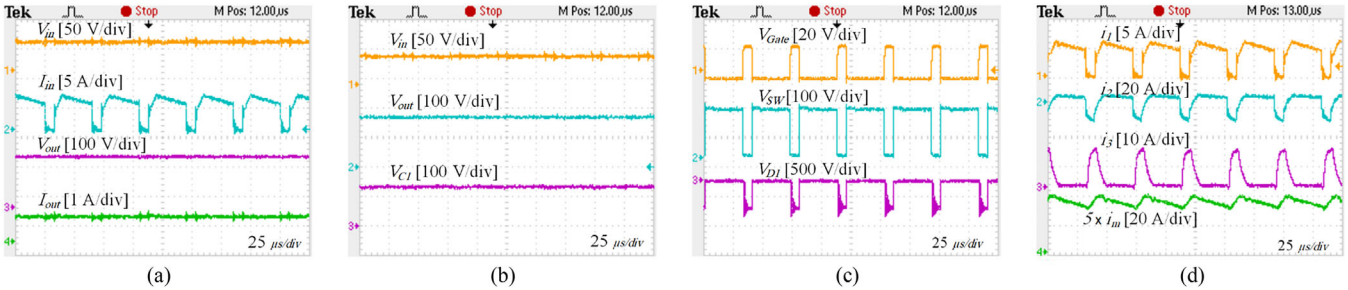

FIGURE 13 YSN experimental results. (a) Input and output voltages and currents, (b) Input, output and capacitor C_1 voltages, (c) ST pulses and blocking voltages of active elements, (d) Windings N_1 to N_3 and magnetizing currents

TABLE 9 Voltage gain comparison between theoretical, simulation and experimental results

Converter		YSN	q-YSN	DA-YSN
Output voltage (V)	Theoretical (ideal)	200	200	200
	Theoretical (non-ideal)	181	184	185
	Simulation	178	181	184
	Experimental	174	180	184

Also, a low capacitors' voltage ripple is measured as almost less than 5%, which is in agreement with the capacitor design equation in Section 3. Obviously, the total capacitor voltage stress of DA-YSN is almost equal to YSN and considerably lower than q-YSN.

The blocking voltages of the switching devices, as well as the gate signal of the switch, are presented in Figures 12–14c. As already expected, in DA-YSN, the switch *SW* and the diode D_2 conduct during the ST state simultaneously, while the diode D_1 blocks. On the contrary, the diode D_1 conducts during the NST state while the diode D_2 and the switch *SW* are open.

Figures 12–14d are the current through the coupled inductor windings and the magnetizing branch. Confirming the theoretical analysis, the coupled inductors are charged during the ST state and discharged during the NST state for all networks, and it happens with a lower ripple for DA-YSN (at the same voltage and power levels).

In order to verify the small-signal calculations, the single-loop PI controller is applied to DA-YSN according to Figure 10 with the same coefficients set in Section 5. To investigate the

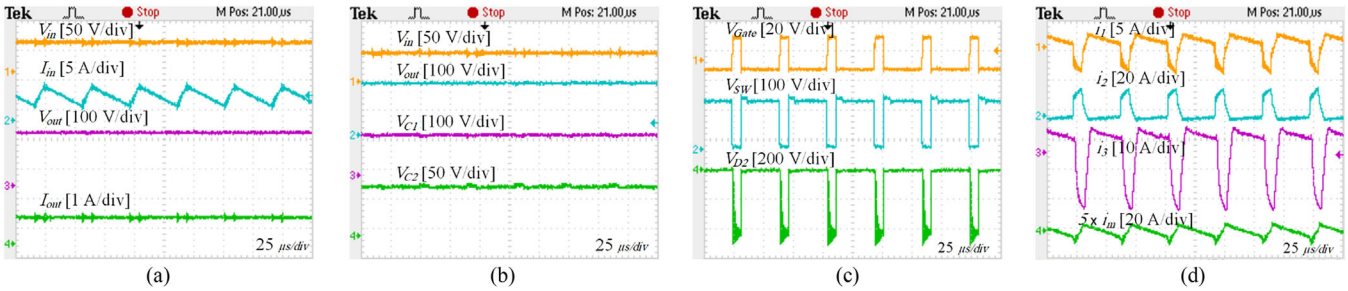

FIGURE 14 q-YSN experimental results. (a) Input and output voltages and currents, (b) Input, output and capacitors C_1 and C_2 voltages, (c) ST pulses and blocking voltages of active elements, (d) Windings N_1 to N_3 and magnetizing currents

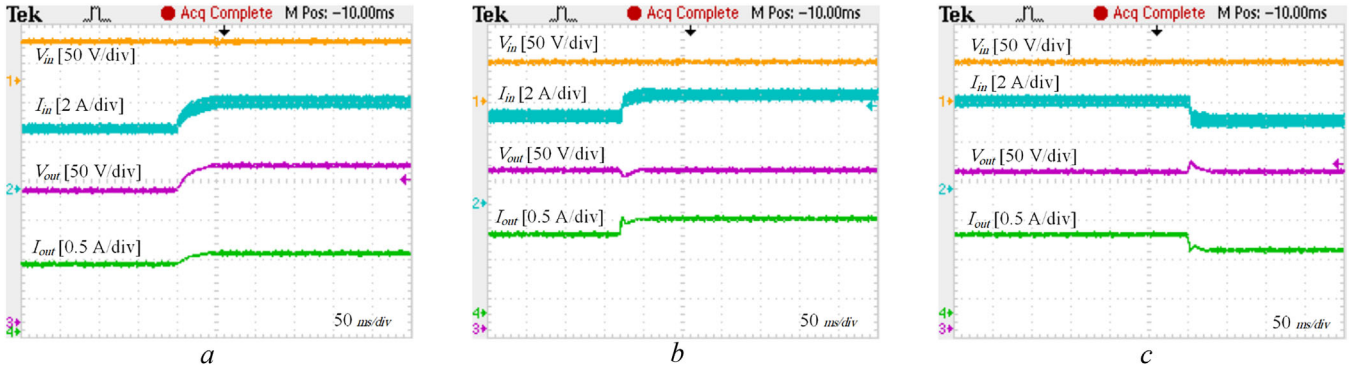

FIGURE 15 Dynamic response of DA-YSN when (a) Voltage reference jumps from 170 to 200 V, (b) Output load jumps from 200 to 240 W, (c) Output load falls from 200 to 160 W

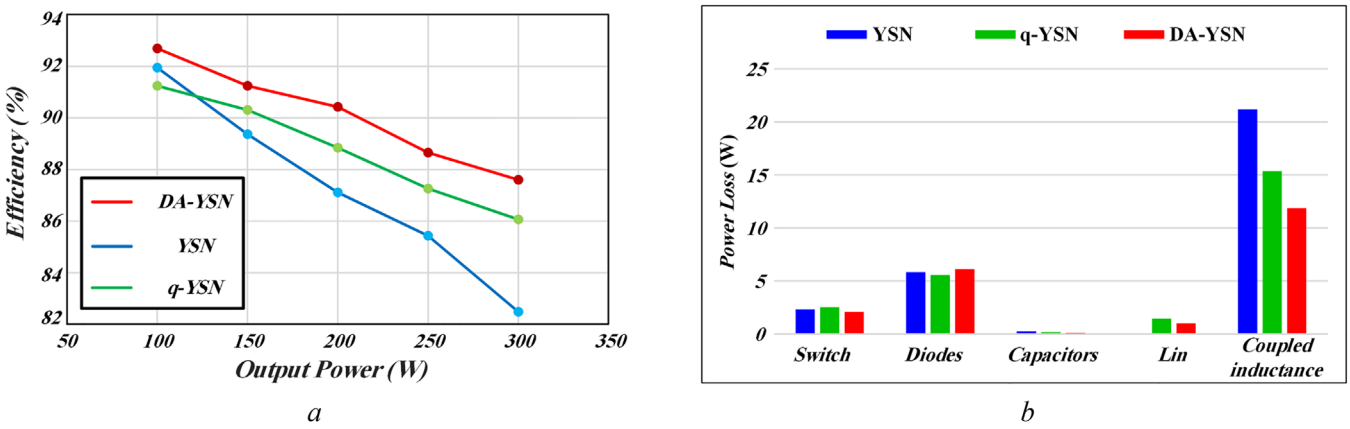

FIGURE 16 (a) Efficiency and (b) Loss distribution comparison

behaviour of the closed-loop system, the reference output voltage is raised from 170 to 200 V, while the input/output voltages and currents are measured and reported in Figure 15a. The fast and smooth transient is obvious as the voltage settles to 200V in less than 50 ms without any overshoot, which in close agreement with the theoretically obtained settling time of 43 ms. Also, to investigate the transient behaviour of DA-YSN in response to the output load step-changes, the closed-loop dynamic responses are depicted in Figure 14. The input/output voltages and currents are measured when the output power is raised (changed from 200 W to 240 W) and decreased (changed from 200 W to 160 W) 20%, and the results are shown in Figure 15b and Figure 15c, respectively. The output reference voltage is 200 V, and it can be seen from these figures that the output voltage is 200 V before step-change, and it is settled to 200 V after almost 30 ms of the transient.

Figure 16a compares the efficiency of all converters for a wide range of output power. The output and input voltages are kept constant at 200 V and 50 V, respectively. At the rated power of 200 W, the efficiencies are 87.11%, 88.85% and 90.43% for YSN, q-YSN and DA-YSN, respectively. It can be concluded from this figure that the efficiency of DA-YSN is the highest. Also, to better investigate the efficiency of the Y-shaped networks, their power loss distributions are analytically calculated based on the method explained in [48] and presented in Figure 16b. Also, the numerical power losses of each component among the Y-shaped networks in Figure 16b are summarized in Table 10. As can be seen from this table, although all networks use the same coupled inductor, DA-YSN offers considerably lower losses in the windings of the coupled inductors than the competitors, as already expected from Table 4. Furthermore, it can also be seen that the power losses of other components of the three networks are approximately equal. In addition, due to the low ESR of the film capacitor used in the experiments, the related power losses are negligible in all networks. Finally, to investigate the effect of the winding factor δ on the power losses of DA-YSN, its efficiency is calculated for various δ at 200 W and the results are shown in Figure 17. For this purpose, the inductors are designed for $\delta = 3$, 4, 5 and 6 and the efficiency is calculated for the input and output voltages of 50 V and 200 V, respectively. As can be seen from Figure 17, the efficiencies for $\delta = 3$ and 4 are almost the same, and the efficiency decreases by increasing the winding factor.

TABLE 10 Power losses of the components at rated power 200 W

				Input inductance		Magnetizing inductance	
Converter	**Switch**	**Diodes**	**Capacitors**	**Core**	**Windings**	**Core**	**Windings**
YSN	2.33 W	5.83 W	0.24 W	NA		0.35 W	20.83 W
q-YSN	2.55 W	5.56 W	0.18 W	0.41 W	1.04 W	0.75 W	14.60 W
DA-YSN	2.07 W	6.11 W	0.12 W	0.01 W	0.98 W	0.34 W	11.5 W

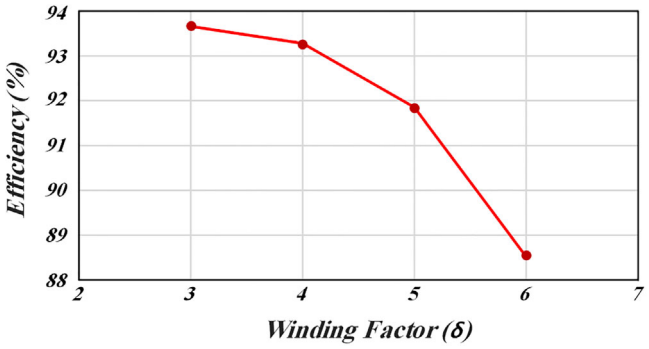

FIGURE 17 Efficiency comparison of DA-YSN vs δ

7 | CONCLUSION

This paper thoroughly investigates the family of diode-assisted impedance source networks, where DA- ΓSN, DA-TSN and DA-F ΓSN are derived by removing one of the windings of DA-YSN and rearranging the remained ones. Therefore, as the basic structure, DA-YSN is analysed and compared with conventional YSN and q-YSN. Accordingly, it offers higher voltage gain with the same $D_{ST,max}$ and significantly lower input current ripple in comparison to the competitors, which are advantageous for renewable energy and high voltage gain applications such as distributed power generation. Lower magnetizing and input current ripples lead to a higher power density of DA-YSN in comparison to q-YSN. Decreased capacitor voltage stress and its value are the other benefits translating to the lower stored energy and volume of DA-ISNs' capacitors. Also, the considerably lower total power loss of the magnetic element compared to that of successful counterparts is the main reason behind the higher efficiency of DA-YSN. Furthermore, to investigate the transient behaviour of DA-YSN and facilitate the controller design procedure, its trasfer functions are derived and a simple single-loop voltage controller is designed to track the output voltage reference. The aforesaid attributes are practically confirmed through extensive tests on a 200 W laboratory setup.

CONFLICT OF INTEREST

The authors declare no conflict of interest.

DATA AVAILABILITY STATEMENT

Data available on request from the authors.

REFERENCES

1. Peng, F.Z., Yuan, X., Fang, X., Qian, Z.: Z-source inverter for adjustable speed drives. IEEE Power Electron. Lett. 1(2), 33–35 (2003)
2. Peng, F.Z., Joseph, A., Wang, J., et al.: Z-source inverter for motor drives. IEEE Trans. Power Electron. 20(4), 857–863 (2005)
3. Zhou, Z.J., Zhang, X., Xu, Po, Shen, W.X.: Single-phase uninterruptible power supply based on Z-source inverter. IEEE Trans. Ind. Electron. 55(8), 2997–3004 (2008)
4. Rymarski, Z., Bernacki, K.: Influence of Z-source output impedance on dynamic properties of single-phase voltage source inverters for uninterrupted power supply. IET Power Electron. 7(8), 1978–1988 (2014)
5. Bansal, R.C., Gitau, M.N., Kala-Konga, C.L.: Steady-state and small-signal models of a three-phase quasi-Z-source AC–DC converter for wind applications. IET Renew. Power Gener. 10(7), 1033–1040 (2016)
6. Karaman, E., Farasat, M., Trzynadlowski, A.M.: Indirect matrix converters as generator–grid interfaces for wind energy systems. IEEE J. Emerg. Sel. Top. Power Electron. 2(4), 776–783 (2014)
7. Li, Y., Jiang, S., Cintron-Rivera, J.G., Peng, F.Z.: Modeling and control of quasi-Z-source inverter for distributed generation applications. IEEE Trans. Ind. Electron. 60(4), 1532–1541 (2013)
8. Siwakoti, Y.P., Loh, P.C., Blaabjerg, F., Andreasen, S.J., Town, G.E.: Y-source boost DC/DC converter for distributed generation. IEEE Trans. Ind. Electron. 62(2), 1059–1069 (2015)
9. Tang, Y., Xie, S., Wei, J.: Grid-tied photovoltaic system with series Z-source inverter. IET Renew. Power Gener. 7(3), 275–283 (2013)
10. Arun, K., Kishor, G.: A high output Y-source boost DC /DC converter for renewable applications. Int. J. Eng. Res. Technol. 9(09), 980–988 (2020)
11. Shen, M., Joseph, A., Wang, J., Peng, F.Z., Adams, D.J.: Comparison of traditional inverters and Z-source inverter for fuel cell vehicles. IEEE Trans. Power Electron. 22(4), 1453–1463 (2007)
12. Guo, F., Fu, L., Lin, C.-H., Li, C., Choi, W., Wang, J.: Development of an 85-kW bidirectional quasi-Z-source inverter with DC-link feed-forward compensation for electric vehicle applications. IEEE Trans. Power Electron. 28(12), 5477–5488 (2013)
13. Peng, F.Z., Shen, M., Holland, K.: Application of Z-source inverter for traction drive of fuel cell—battery hybrid electric vehicles. IEEE Trans. Power Electron. 22(3), 1054–1061 (2007)
14. Corzine, K.A., Ashton, R.W.: A new Z-source DC circuit breaker. IEEE Trans. Power Electron. 27(6), 2796–2804 (2012)
15. Siwakoti, Y.P., Peng, F.Z., Blaabjerg, F., Loh, P.C., Town, G.E., Yang, S.: Impedance-source networks for electric power conversion part II: Review of control and modulation techniques. IEEE Trans. Power Electron. 30(4), 1887–1906 (2015)
16. Duong, T., Nguyen, M., Lim, Y., Choi, J., Vilathgamuwa, D.M.: SiC-based active quasi-Z-source inverter with improved PWM control strategy. IET Power Electron. 12(14), 3810–3821 (2019)
17. Wang, R., Han, X., Liu, C., Zhao, Y., Zhang, J.: Carrier-based PWM control strategy for Z -source two-stage matrix converter. IET Power Electron. 12(13), 3527–3538 (2019)
18. Pilehvar, M.S., Mardaneh, M.: Phase-shift control and harmonics elimination for H-bridge Z-source inverter. IET Power Electron. 8(4), 618–627 (2015)
19. Barathy, B., Kavitha, A., Viswanathan, T.: Effective space vector modulation switching sequence for three phase Z source inverters. IET Power Electron. 7(11), 2695–2703 (2014)

20. Gajanayake, C.J., Luo, F.L., Gooi, H.B., So, P.L., Siow, L.K.: Extended-boost Z-source inverters. IEEE Trans. Power Electron. 25(10), 2642–2652 (2010)
21. Nguyen, M., Duong, T., Lim, Y.-C., Kim, Y.: Switched-capacitor quasi-switched boost inverters. IEEE Trans. Ind. Electron. 65(6), 5105–5113 (2018)
22. Sharifi, S., Monfared, M.: Modified series and tapped switched-coupled-inductors quasi-Z-source networks. IEEE Trans. Ind. Electron. 66(8), 5970–5978 (2019)
23. Sharifi, S., Chulaee, Y., Abootorabi, H., Monfared, M.: Generalized three-winding switched-coupled-inductor impedance networks with highly flexible gain. IEEE Trans. Ind. Electron. 0046(c), 1–1 (2020)
24. Hosseini, S.M., Ghazi, R., Nikbahar, A., Eydi, M.: A new enhanced-boost switched-capacitor quasi-Z-source network. IET Power Electron. 14(2), 412–421 (2021)
25. Hasan Babayi Nozadian, M., Babaei, E., Hosseini, S.H.: Shokati Asl, E.: Switched Z-source networks: A review. IET Power Electron. 12(7), 1616–1633 (2019)
26. Asl, E.S., Babaei, E., Sabahi, M.: High voltage gain half-bridge quasi-switched boost inverter with reduced voltage stress on capacitors. IET Power Electron. 10(9), 1095–1108 (2017)
27. Li, L., Tang, Y.: A high set-up quasi-Z-source inverter based on voltage-lifting unit. In: 2014 IEEE Energy Conversion Congress and Exposition (ECCE), pp. 1880–1886. IEEE (2014)
28. Siwakoti, Y.P., Loh, P.C., Blaabjerg, F., Town, G.E.: Y-source impedance network. IEEE Trans. Power Electron. 29(7), 3250–3254 (2014)
29. Loh, P.C., Blaabjerg, F.: Magnetically coupled impedance-source inverters. IEEE Trans. Ind. Appl. 49(5), 2177–2187 (2013)
30. Hakemi, A., Sanatkar-Chayjani, M., Monfared, M.: Δ-source impedance network. IEEE Trans. Ind. Electron. 64(10), 7842–7851 (2017)
31. Soon, J.J., Low, K.-S.: Sigma-Z-source inverters. IET Power Electron. 8(5), 715–723 (2015)
32. Siwakoti, Y.P., Blaabjerg, F., Loh, P.C.: Quasi-Y-source boost DC–DC converter. IEEE Trans. Power Electron. 30(12), 6514–6519 (2015)
33. Siwakoti, Y.P., Blaabjerg, F., Loh, P.C.: New magnetically coupled impedance (Z-) source networks. IEEE Trans. Power Electron. 31(11), 7419–7435 (2016)
34. Ayachit, A., Siwakoti, Y.P., Galigekere, V.P.N., Kazimierczuk, M.K., Blaabjerg, F.: Steady-state and small-signal analysis of A-source converter. IEEE Trans. Power Electron. 33(8), 7118–7131 (2018)
35. Rezazadeh, H., Monfared, M., Nikbahar, A., Sharifi, S.: A family of high voltage gain quasi-Δ-source impedance networks. IET Power Electron. 14(4), 807–820 (2021)
36. Rezazadeh, H., Monfared, M.: Quadratic Δ-source impedance network. In: 2020 11th Power Electronics, Drive Systems, and Technologies Conference (PEDSTC), pp. 1–5. IEEE (2020)
37. Siwakoti, Y.P., Loh, P.C., Blaabjerg, F., Town, G.E.: Effects of leakage inductances on magnetically coupled Y-source network. IEEE Trans. Power Electron. 29(11), 5662–5666 (2014)
38. Liu, H., Zhou, Z., Liu, K., et al.: A family of high step-up coupled-inductor impedance-source inverters with reduced switching spikes. IEEE Trans. Power Electron. 33(11), 9116–9121 (2018)
39. Reddivari, R., Jena, D., Gautham, T.N.: Analysis, design, and performance evaluation of differential-mode Y-source converters for voltage spikes mitigation. IEEE Trans. Ind. Appl. 56(6), 6701–6710 (2020)
40. Anderson, J., Peng, F.Z.: Four quasi-Z-source inverters. In: 2008 IEEE Power Electronics Specialists Conference, pp. 2743–2749. IEEE (2008)
41. Forouzesh, M., Siwakoti, Y.P., Blaabjerg, F., Hasanpour, S.: Small-signal modeling and comprehensive analysis of magnetically coupled impedance-source converters. IEEE Trans. Power Electron. 31(11), 7621–7641 (2016)
42. Kong, X., Wong, C., Lam, C.: Effects of parasitic resistances on magnetically coupled impedance-source networks. IEEE Trans. Power Electron. 35(9), 9171–9183 (2020)
43. Liu, H., Zhou, Z., Liu, K., et al.: High step-up Y-source inverter with reduced DC-link voltage spikes. IEEE Trans. Power Electron. 34(6), 5487–5499 (2019)
44. Wijeratne, D.S., Moschopoulos, G.: Quadratic power conversion for power electronics: Principles and circuits. IEEE Trans. Circuits Syst. I Regul. Pap. 59(2), 426–438 (2012)
45. Mclyman, C.W.: Transformer and Inductor Design Handbook. CRC Press, Boca Raton (2011)
46. Magnetics Powder Core Catalog. (2015). [Online]. www.mag-inc.com
47. Åström, K., Hägglund, T.: Advanced PID control. ISA–The Instrumentation, Systems, and Automation Society, Research Triangle Park, NC (2005)
48. Nguyen, M.-K., Lim, Y.-C., Park, S.-J.: Improved trans-Z-source inverter with continuous input current and boost inversion capability. IEEE Trans. Power Electron. 28(10), 4500–4510 (2013). Last accessed 2018

How to cite this article: Rezazadeh, H., Monfared, M., Nikbahar, A.: Modelling and performance evaluation of diode-assisted impedance source networks. IET Power Electron. 1–15 (2021). https://doi.org/10.1049/pel2.12201